American Mineralogist, Volume 93, pages 1911–1920, 2008

Xocolatlite, $Ca_2Mn_2^{4+}Te_2O_{12}\cdot H_2O$, a new tellurate related to kuranakhite: Description and measurement of Te oxidation state by XANES spectroscopy

Pascal V. Grundler,[1,*] Joël Brugger,[1] Nicolas Meisser,[2] Stefan Ansermet,[2] Stacey Borg,[3] Barbara Etschmann,[3] Denis Testemale,[4] and Trudy Bolin[5]

[1]Department of Geology and Geophysics, University of Adelaide, North Terrace, SA-5005 Adelaide, Australia and South Australian Museum, North Terrace, SA-5000 Adelaide, Australia
[2]Musée Cantonal de Géologie and Laboratoire des Rayons-X, Institut de Minéralogie and Géochimie, UNIL-Anthropole, CH-1015 Lausanne-Dorigny, Switzerland
[3]CSIRO Exploration and Mining, Clayton, VIC-3800, Australia
[4]CNRS Institut Néel, département MCMF, 25 Avenue des Martyrs, 38042 Grenoble Cedex 9, France and SNBL/ESRF, 6 Rue Jules Horowitz, 38043 Grenoble, France
[5]Advanced Photon Source, Sector 9 BM, Argonne, Illinois 60439, U.S.A.

Abstract

Xocolatlite, $Ca_2Mn_2^{4+}Te_2^{6+}O_{12}\cdot H_2O$, is a rare new mineral from the Moctezuma deposit in Sonora, Mexico. It occurs as chocolate-brown crystalline crusts on a quartz matrix. Xocolatlite has a copper-brown streak, vitreous luster, and is transparent. Individual crystals show a micaceous habit. Refractive indices were found to be higher than 2.0. Density calculated from the empirical formula is 4.97 g/cm^3, and immersion in Clerici solution indicated a density higher than 4.1 g/cm^3. The mineral is named after the word used by the Aztecs for chocolate, in reference to its brown color and provenance.

The crystallographic characteristics of this monoclinic mineral are space group *P*2, *P*2/*m*, or *Pm*, with the following unit-cell parameters refined from synchrotron X-ray powder diffraction data: a = 10.757(3) Å, b = 4.928(3) Å, c = 8.942(2) Å, β = 102.39(3)°, V = 463.0(3) Å^3, and Z = 2. The unavailability of a suitable crystal prevented single-crystal X-ray studies. The strongest 10 lines of the X-ray powder diffraction pattern are [d in Å (I) (hkl)]: 3.267(100)(012), 2.52(71)(30$\bar{3}$), 4.361(51)(002), 1.762(39)(32$\bar{3}$), 4.924 (34)(010), 2.244(32)(31$\bar{3}$), 1.455(24)(006), 1.996(21)(014), 1.565(20)(611), and 2.353(18)(41$\bar{1}$).

XANES Te L_{III}-edge spectra of a selection of Te minerals (including xocolatlite) and inorganic compounds showed that the position of the absorption edge can be reliably related to the oxidation state of Te. XANES demonstrated that xocolatlite contains Te^{6+} as a tellurate group. Water has been tentatively included in the formula based on IR spectroscopy that indicated the presence of a small amount of water. Raman, IR, XANES, and X-ray diffraction data together with the chemical composition show a similarity of xocolatlite to kuranakhite. A possible series may exist between these two species, xocolatlite being the Ca-rich end-member and kuranakhite the Pb-rich one.

Keywords: Xocolatlite, Kuranakhite, new mineral, XANES spectroscopy, tellurium oxidation state, Moctezuma, Sonora, Mexico

Introduction

Despite low crustal abundances (1 ppb, compared to 3.1 ppb for Au), the semi-metal tellurium (Te) is found in relatively high concentrations (tens to thousands of ppm) in several ore deposits. In particular, Te is closely associated with Au in many epithermal-type deposits such as Cripple Creek, Colorado (Kelley et al. 1998), Emperor, Fiji (Pals and Spry 2003), and Săcărîmb, Romania (Ciobanu et al. 2004), as well as in some "orogenic" gold deposits, including the giant Golden Mile deposit and the world-class Sunrise Dam deposit in Western Australia (Bateman and Hagemann 2004; Shackleton et al. 2003; Sung et al. 2007). Tellurium mineralogy tends to be relatively complex, with more than 140 minerals containing Te as an essential element known worldwide. This complexity is linked primarily to the rich redox chemistry of Te, where many oxidation states are available for this element: Te^{6+}, Te^{4+}, Te^0, Te^{2-} as well as intermediate states such as in polytellurides (e.g., Te_2^{2-}).

The Moctezuma deposit in Sonora, Mexico, can be considered as the "World Capital" of tellurium mineralogy. Moctezuma is the type locality for 22 known minerals, all containing Te (Braith et al. 2001). Three of those minerals are tellurides (bambollaite, benleonardite, cervelleite), corresponding to primary hydrothermal minerals. The rest are tellurites (Te^{4+}) and tellurates (Te^{6+}) that developed during weathering of the deposit. In this

* E-mail: pascal.grundler@adelaide.edu.au or pascal.grundler@a3.epfl.ch

communication we describe a new mineral, xocolatlite, discovered recently on the dumps of the Moctezuma deposit. We also illustrate how X-ray absorption near edge structure (XANES) spectroscopy can be used to measure the oxidation state of Te in minerals and other inorganic materials.

Mineral name and type material

The new mineral and its name have been approved by the Commission on New Minerals, Nomenclature and Classification (IMA 2007-20). The new mineral name is derived from the Náhuatl (the language spoken by the Aztecs) word xocolatl or xocoatl, meaning "bitter water" (xoc = bitter, atl = water) and used to indicate a sacred beverage made by mixing cocoa, water, vanilla, pepper, and chili. The Náhuatl name is the root of all European words for this preparation, as chocolate (English, Spanish), Schokolade (German), chocolat (French), chocolade (Dutch), cioccolata (Italian), choklad (Swedish), suklaa (Finnish), and шоколад (Russian). Xocolatlite is named in allusion to its chocolate-brown color, its Mexican type locality, and to continue the tradition of using Aztec-related words for the Moctezuma minerals, with such exquisite examples as quetzalcoatlite, tlapallite, tlalocite, and xocomecatlite. "Xocolatl" is preferred over "xocoatl" because the former forms the root in many European languages, and xocolatlite is easier to pronounce in English.

Type material is deposited in the Musée Cantonal de Géologie, Lausanne, Switzerland. Holotype specimen is MGL90740.

Occurrence, associated minerals, and origin

The mineral occurs in the Bambolla mine (29°41′N 109°42′W, alt. 830 m), Moctezuma, Sonora, Mexico. The tellurite/tellurate minerals of this deposit formed as the result of the weathering of an epithermal quartz-tellurium-gold vein system (Deen and Atkinson 1988). The main primary Te-mineral in the vein is native tellurium, with a few tellurides occurring as minor components.

Xocolatlite is found associated with quartz, barite, jarosite, emmonsite (Te^{4+}), and on some samples also with schmitterite (Te^{4+}) and eztlite (Te^{4+} and Te^{6+}). The samples investigated here were collected on dumps in 2002.

Appearance, physical, and optical properties of xocolatlite

The new mineral is extremely rare (<10 specimens recorded) and occurs as brown crystalline crusts on a quartz matrix showing dissolution textures (Fig. 1). The crusts are formed of micaceous plates, with individual crystals having a maximum length of ~40 μm (Fig. 1b). The resulting crusts are up to 200 μm thick; in section, they show growth banding, and evidence for formation as a gel-like material (Fig. 1a). No twinning has been observed.

The mineral shows a chocolate-brown color (RAL 8017, Deutsches Institut für Gütesicherung und Kennzeichnung e. V., D-53757 Sankt Augustin, http://www.ral.de) and has copper-brown streak (RAL 8004). Its luster is vitreous, and it is transparent. No fluorescence has been observed. The Mohs hardness is between 2 and 3 and the mineral is brittle. It shows a perfect mica-like cleavage and a conchoidal fracture. Immersion in Clerici solution showed that the density is higher than

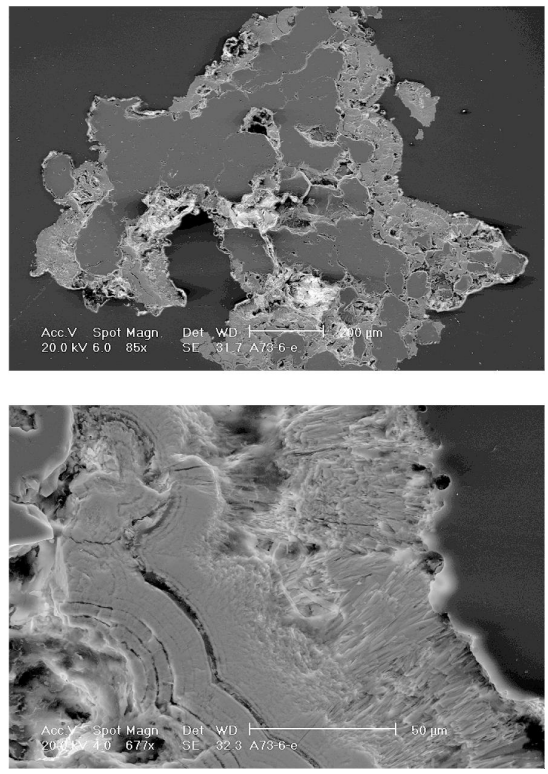

Figure 1. Scanning electron microscope images of xocolatlite from Moctezuma (secondary electron mode; holotype sample MGL90740). (**a**) Overgrowth of xocolatlite on corroded quartz. (**b**) Close-up view, showing gel-like texture in xocolatlite at the contact with quartz, and micaceous (section is near-perpendicular to plate orientation) crystals up to about 40 μm in length on the outside.

4.1 g/cm^3. Some grains had an apparent density of about 4.04 g/cm^3; however, they were porous and air bubbles escaped upon crushing them. The density calculated from the empirical formula (see below) is 4.97 g/cm^3. Using an anhydrous empirical formula yields a slightly lower value for the density at 4.84 g/cm^3. The density calculated from the ideal formula is 4.70 g/cm^3. All these values are in agreement with the result obtained using the heavy liquid.

Xocolatlite is non-pleochroic. By immersion in refractive index oils, the refractive indices of xocolatlite were found to be higher than 2.0. These high values, as well as habit and crystal size, prevented accurate optical studies.

Crystallography

The powder-diffraction pattern was recorded using synchrotron radiation (λ = 0.50067 Å) at the Swiss-Norwegian beamline (SNBL) at the European Synchrotron Research Facility (ESRF), using their high-resolution powder diffraction instrument. Quartz, present as a contaminant in the sample, was used as an internal standard. Single-crystal X-ray studies could not be carried out because no suitable crystal was available. An attempt to use microcrystals at the ESRF failed due to the poor quality of the reflections.

The unit cell was obtained using the program DicVol91

(Boultif and Louer 1991), using all 35 lines observed on the synchrotron powder pattern (Table 1). Xocolatlite was determined to be monoclinic with unit-cell parameters: a = 10.757(3) Å, b = 4.928(3) Å, c = 8.942(2) Å, β = 102.39(3)°, V = 463.0(3) Å^3, and Z = 2. Based on lack of systematic extinctions, xocolatlite belongs to either the space group $P2$, $P2/m$, or Pm.

Chemical composition

The chemistry of xocolatlite was investigated in 23 chemical analyses, which were carried out by means of a CAMECA SX51 electron microprobe operated in WDS mode, 15 kV, 20 nA, ~1 µm beam diameter; counting times of 10 s on the peak and 5 s on each side of the peak for background. The following X-ray lines and standards were used: Te$L\alpha$, synthetic paratellurite TeO_2; Bi$M\alpha$ and Se$L\alpha$, synthetic Bi_2Se_3; S$K\alpha$, barite; Al$K\alpha$ and Si$K\alpha$, almandine; Ca$K\alpha$, wollastonite; Mn$K\alpha$, rhodonite; Zn$K\alpha$, ZnS; Cd$L\alpha$, Cd metal; Pb$M\alpha$, crocoite. The analyzed samples include the holotype MGL90740 as well as two other xocolatlite samples (MGL90738 and MGL90739) and a sample of kuranakhite (MGL90744) from Moctezuma (respectively, 23, 20, 31, and 22 analyses). The low analytical sums for the holotype appear to be related to sample texture; the material is fibrous/micaceous and may include porosity as well as some amorphous "Te ochre." The analytical total for MGL90739 and MGL90744, which are characterized by more compact textures, are closer to 100%.

Results are shown in Table 2 and in Figure 2. In addition to the main constituents Te, Ca, and Mn, xocolatlite contains small quantities of Al (up to 2.34 wt% Al_2O_3), Fe (up to 9.92 wt% Fe_2O_3), Zn (up to 2.47 wt% ZnO), and Pb (up to 5.85 wt% PbO), as well as trace amounts of As (≤0.1 wt% As_2O_5), Se (≤0.16 wt% SeO_3), Cd (≤0.42 wt% CdO), Cu (≤0.9 wt% CuO), and Bi (≤0.37 wt% Bi_2O_3). Varying amounts of Si (up to 2.14 wt% SiO_2) are probably a contamination from finely dispersed quartz in the sample. No other element with atomic number >9 was detected. Xocolatlite MGL90738 is characterized by varying amounts of Fe (Figs. 2a, 2b, and 2e), while MGL90739 and MGL90740 have higher Mn contents (Fig. 2c). All analyzed xocolatlite specimens have low Pb content. In contrast, the main chemical variability in kuranakhite sample MGL 90744 is the substitution of Pb by Ca (Figs. 2d and 2e).

Infrared (IR) and laser Raman spectra of xocolatlite and a set of tellurium minerals were measured. In particular, we aimed to check for the presence of structural water in xocolatlite (Fig. 3), and to compare xocolatlite with the related mineral kuranakhite (Fig. 4). Over the 100–700 cm^{-1} spectral range, IR spectra were recorded on a Bruker IFS 113v FT spectrometer. A few milligrams of mineral powder were ground together with polyethylene (Uvasol, Merck) and pressed into a disk. Spectra were recorded under vacuum. A Perkin Elmer SpectrumOne spectrometer equipped with an ATR accessory was used to record spectra from 650 to 4000 cm^{-1}. No special sample preparation was required; a few milligrams of mineral sample were simply pressed onto the diamond crystal of the ATR accessory. Laser Raman spectra were recorded in the range from 3800 to 100 cm^{-1} with a Renishaw Ramascope 1000 using an argon laser (488 nm line) and excitation through a Leica DMLM optical microscope (Si standard, spectral resolution 2 cm^{-1}, unpolarized laser light, random sample orientation).

Table 1. Synchrotron X-ray powder-diffraction data for xocolatlite

d_{obs}	d_{calc}	Diff 2θ	I_{obs}	$h\,k\,l$
4.998	5.000	0.003	5.6	2 0 $\bar{1}$
4.924	4.929	0.005	34.2	0 1 0
4.361	4.367	0.009	50.7	0 0 2
3.267	3.268	0.004	100.0	0 1 2
3.034	3.034	–0.001	1.4	3 0 1
2.52	2.520	0.001	71.2	3 0 $\bar{3}$
2.464	2.464	0.001	2.0	0 2 0
2.353	2.354	0.003	17.8	4 1 $\bar{1}$
2.244	2.244	–0.001	31.5	3 1 $\bar{3}$
2.182	2.183	0.009	2.6	0 0 4
2.146	2.146	0.001	1.7	0 2 2
	2.142	–0.024		4 1 1
	2.148	0.010		1 2 $\bar{2}$
2.038	2.036	–0.015	5.6	1 1 $\bar{4}$
1.996	1.996	0.002	20.9	0 1 4
1.777	1.775	–0.014	6.2	2 0 $\bar{5}$
1.762	1.762	0.000	38.8	3 2 $\bar{3}$
	1.761	–0.009		6 0 $\bar{2}$
1.650	1.651	0.011	4.5	5 1 2
	1.650	0.001		6 0 1
	1.650	0.001		6 1 0
1.634	1.634	0.002	2.6	0 2 4
1.565	1.565	–0.003	20.1	6 1 1
1.455	1.456	0.008	24.0	0 0 6
	1.456	0.007		7 1 $\bar{2}$
1.441	1.441	–0.007	3.9	2 2 $\bar{5}$
1.396	1.396	0.000	6.6	0 1 6
1.313	1.313	–0.004	2.1	0 3 4
	1.313	0.006		8 0 0
1.260	1.260	0.002	6.3	6 0 $\bar{6}$
1.253	1.253	0.005	5.3	0 2 6
	1.252	–0.013		3 0 6
1.221	1.220	–0.019	3.7	0 4 1
	1.222	0.025		4 2 $\bar{6}$
	1.221	–0.006		5 0 5
	1.221	–0.003		6 1 $\bar{6}$
	1.220	–0.012		8 1 1
1.211	1.212	0.015	2.0	8 1 $\bar{4}$
	1.211	0.004		6 3 $\bar{1}$
1.177	1.176	–0.017	8.1	5 2 $\bar{6}$
	1.177	–0.004		8 2 $\bar{2}$
1.164	1.163	–0.021	2.3	3 4 $\bar{1}$
	1.164	0.005		6 3 1
1.122	1.122	0.004	6.7	6 0 $\bar{5}$
	1.122	–0.001		6 2 $\bar{6}$
	1.122	0.003		6 3 $\bar{4}$
1.107	1.107	–0.002	1.8	3 4 $\bar{3}$
	1.107	–0.005		9 1 $\bar{4}$
1.092	1.092	–0.007	1.2	0 0 $\bar{8}$
	1.091	–0.020		3 3 $\bar{6}$
	1.091	–0.020		3 3 $\bar{6}$
	1.092	–0.002		5 0 6
1.066	1.066	–0.003	1.7	0 1 $\bar{8}$
	1.067	0.024		5 0 $\bar{8}$
	1.066	0.002		5 1 6
	1.066	0.006		1 3 $\bar{6}$
1.001	1.001	0.002	1.2	3 4 $\bar{5}$
	1.000	–0.015		4 2 $\bar{8}$
	1.000	–0.015		4 2 $\bar{8}$
	1.001	0.002		3 4 $\bar{5}$
0.982	0.981	–0.019	3.3	1 5 0
	0.981	–0.019		1 5 0
	0.982	0.001		10 2 $\bar{1}$
	0.982	–0.013		4 4 $\bar{5}$
0.953	0.954	0.020	3.4	4 3 6
	0.952	–0.021		7 4 0
	0.953	0.016		7 2 5
	0.953	0.013		11 0 $\bar{4}$
	0.953	0.002		11 1 $\bar{3}$
	0.953	0.014		1 5 2

Comparison of the IR spectra of xocolatlite with IR spectra reported for hydrated tellurites/tellurates (Miletich 1995; Roberts et al. 1994, 1995, 1996a, 1996b, 1997) shows that the weak

TABLE 2. Electron-microprobe analyses of xocolatlite and kuranakhite from Moctezuma, Sonora, Mexico

Mineral	Xocolatlite			Xocolatlite			Xocolatlite			Kuranakhite		
Sample	Type MGL90740			MGL90738			MGL90739			MGL90744		
n	23			20			31			22		
	Mean	Min	Max	Mean	Min	Max	Mean	Min	Max	Mean	Min	Max
						Oxides (wt%)						
TeO_3	48.60	46.64	50.59	51.31	49.00	53.04	51.93	49.88	55.10	37.35	36.02	40.98
SeO_3	0.03	<0.05	0.16	0.04	<0.05	0.13	0.03	<0.05	0.13	0.03	<0.05	0.12
SO_3	0.11	<0.05	0.22	0.24	0.10	0.36	0.09	<0.05	0.24	0.02	<0.05	0.13
SiO_2	1.10	0.47	2.14	0.04	<0.05	0.07	<0.05	<0.05	0.05	<0.05		<0.05
CaO	9.74	9.10	10.46	9.25	7.53	13.33	11.65	7.24	15.41	1.79	0.69	4.83
Al_2O_3	0.28	0.15	0.41	1.99	1.59	2.34	1.05	0.72	1.91	0.10	<0.05	0.42
MnO_2	28.15	25.92	30.20	22.01	19.96	24.30	28.30	14.96	32.46	18.35	17.29	20.70
Fe_2O_3	0.04	<0.04	0.20	6.93	2.97	9.92	0.32	<0.04	8.79	<0.04		<0.05
ZnO	2.16	1.78	2.47	0.83	0.43	1.16	1.30	0.49	2.73	0.08	<0.05	0.18
CdO	0.07	<0.05	0.18	0.12	<0.05	0.25	0.09	<0.05	0.42	0.04	<0.05	0.16
PbO	3.62	1.49	5.39	1.61	1.07	2.18	2.75	1.01	5.85	39.36	28.26	43.96
Bi_2O_3	0.08	<0.05	0.37	0.08	<0.05	0.31	0.05	<0.05	0.23	0.05	<0.05	0.16
H_2O*	2.48	2.39	2.56	2.58	2.48	2.65	2.66	2.46	2.76	1.91	1.84	2.10
Sum	96.46†	94.68	99.15	97.03	93.72	99.17	100.22	95.71	101.8	99.08	96.62	100.75
						Atoms per formula unit						
Te	2.011	1.960	2.061	2.042	1.994	2.098	2.006	1.945	2.125	2.006	1.975	2.031
Se	0.002		0.009	0.002		0.007	0.002		0.007	0.002		0.009
S	0.010		0.020	0.021	0.009	0.032	0.008		0.020			<0.015
Sum	2.02	1.97	2.08	2.07	2.02	2.12	2.02	1.96	2.15	2.01	1.97	2.03
Ca	1.262	1.186	1.319	1.153	0.960	1.613	1.409	0.920	1.807	0.301	0.118	0.741
Al	0.040	0.022	0.061	0.273	0.214	0.319	0.140	0.094	0.251	0.018		0.071
Mn	2.353	2.250	2.523	1.769	1.619	1.914	2.208	1.262	2.529	1.990	1.945	2.047
Fe	0.004		0.019	0.606	0.252	0.867	0.027		0.807			
Zn	0.193	0.165	0.214	0.071	0.036	0.098	0.108	0.040	0.246	0.009	0.000	0.019
Cd	0.004	0.000	0.010	0.006	0.000	0.014	0.005		0.023	0.003		0.011
Pb	0.118	0.048	0.182	0.050	0.033	0.068	0.083	0.030	0.187	1.663	1.088	1.897
Bi	0.002		0.012	0.002		0.009	0.002		0.006	0.002		0.007
Sum	3.976	3.916	4.032	3.934	3.876	3.984	3.984	3.851	4.042	3.988	3.966	4.025
H*	2.0			2.0			2.0			2.0		
O	13.4	13.4	13.5	13.3	13.1	13.4	13.3	13.0	13.7	13.0	12.9	13.1

Note: Normalization based on 6 cations pfu, excluding SiO_2, which is considered to be a contamination from quartz (Fig. 1), significant only in the type specimen MGL90740.

* Water contents calculated assuming 2 H atoms per formula unit.

† Total is low due to empty interstices between the thin xocolatlite fibers and porosity (Fig. 1b).

absorbance bands at 3212 cm^{-1} (O-H stretching) and 1641 cm^{-1} (H-O-H bending) are indicative of the presence of water, but only as a minor component (Fig. 3). Further the bands at 988/928 cm^{-1} may be assigned to O-H···O bending (Novak 1974). This suggests that the water is more than just absorbed on the surface and may be actually part of the crystal structure through hydrogen bonding. Similar bands at slightly higher wavenumbers (1000–1100 cm^{-1}) are found in other hydrated tellurates (mcalpineite, Roberts et al. 1994; leisingite, Roberts et al. 1996b; juabite, Roberts et al. 1997), however they were not assigned to any precise structural feature. Unfortunately the quality of the data are insufficient to quantify the amount of water present using the calibration curve given by (Libowitzky and Rossman 1997). Furthermore, the small amount of material available prevented a direct determination of water by thermogravimetry.

The bands found in the range 100–1000 cm^{-1} correspond to the metal oxygen bonds (Ferraro 1971). The IR and Raman spectra of kuranakhite and xocolatlite are very similar (Fig. 4), indicating a close structural relationship. By analogy to IR and Raman data reported for the synthetic tellurate Ba_2ZnTeO_6 (Liegeois-Duyckaerts 1975), the following tentative assignments are proposed for the Raman spectra of xocolatlite and kuranakhite, respectively (Fig. 4): 699 and 677 cm^{-1} as ν_1 (Te-O symmetric stretch), 630 and 619 cm^{-1} as ν_2 (Te-O symmetric stretch), 390 and 380 cm^{-1} as ν_5 (O-Te-O bending). For the IR spectrum of xocolatlite shown in Figure 3: 746/688 cm^{-1} as ν_3 (O-Te-O bending); IR spectra of xocolatlite and kuranakhite, respectively (Fig. 4): 534/497 and 532/493 cm^{-1} as ν_4 (Te-O asymmetric stretch). A definitive assignment of the bands will have to await the solving of the crystal structure.

MEASURING OXIDATION STATE OF TE BY X-RAY ABSORPTION SPECTROSCOPY

XANES spectra are proportional to the unoccupied density of states (projected on the absorbing atom, in this case Te) and hence reflect the local short- and intermediate-range structure as well as the oxidation state of the central atom. TeO_2 glasses are of enormous technological interest due in part to their non-linear optical properties, and XANES spectroscopy has been applied to study changes in short- to intermediate-range order around Te^{4+} ions in TeO_2-based glasses upon addition of other oxides (Charton and Armand 2004). However, we are not aware of any application of XANES spectroscopy to the study of minerals. The method is attractive because it requires only small sample quantities, down

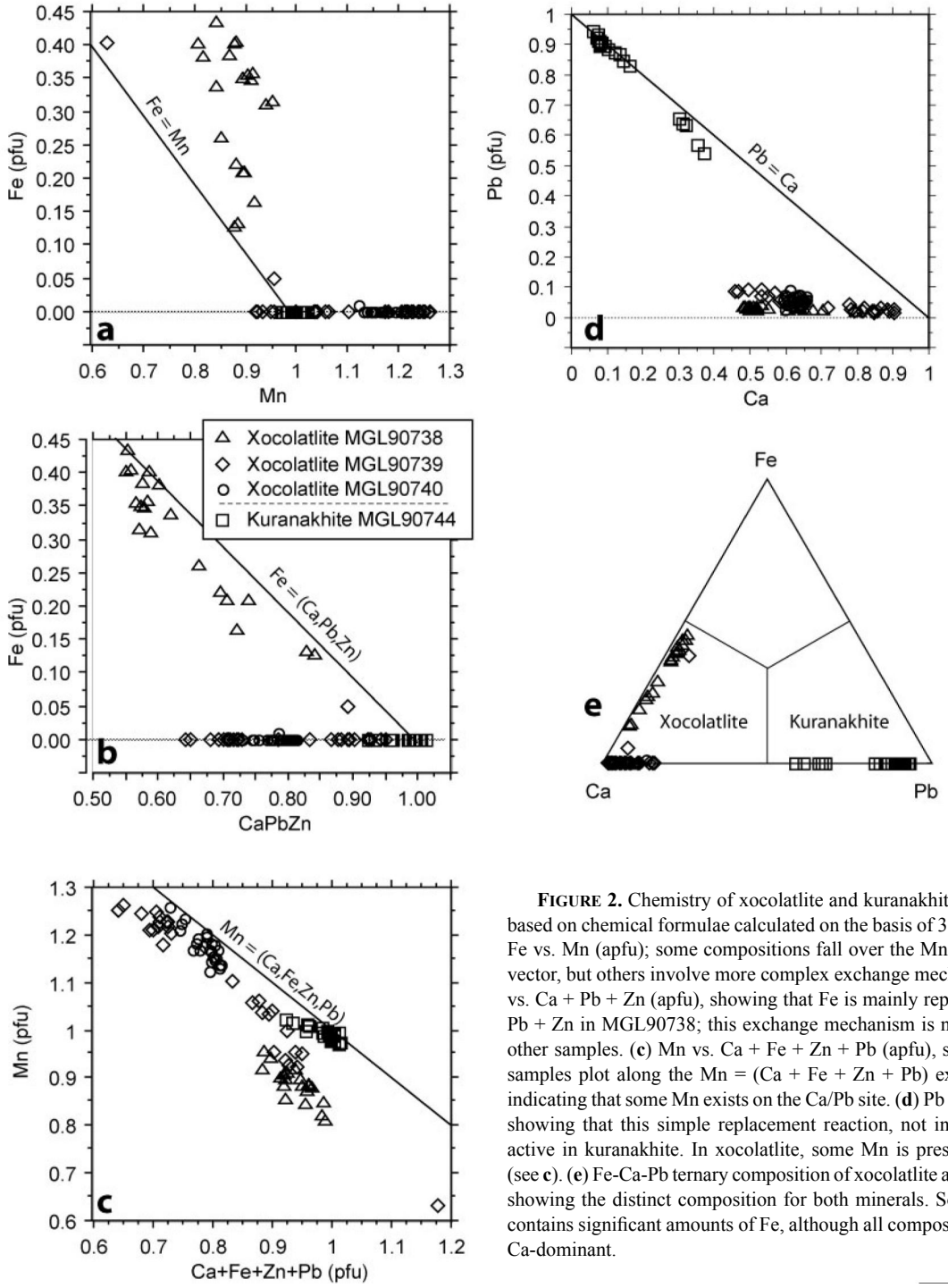

FIGURE 2. Chemistry of xocolatlite and kuranakhite (see Table 2), based on chemical formulae calculated on the basis of 3 cations pfu. (**a**) Fe vs. Mn (apfu); some compositions fall over the Mn = Fe exchange vector, but others involve more complex exchange mechanisms. (**b**) Fe vs. Ca + Pb + Zn (apfu), showing that Fe is mainly replacing the Ca + Pb + Zn in MGL90738; this exchange mechanism is not active in the other samples. (**c**) Mn vs. Ca + Fe + Zn + Pb (apfu), showing that all samples plot along the Mn = (Ca + Fe + Zn + Pb) exchange vector, indicating that some Mn exists on the Ca/Pb site. (**d**) Pb vs. Ca diagram, showing that this simple replacement reaction, not involving Mn, is active in kuranakhite. In xocolatlite, some Mn is present on this site (see **c**). (**e**) Fe-Ca-Pb ternary composition of xocolatlite and kuranakhite, showing the distinct composition for both minerals. Some xocolatlite contains significant amounts of Fe, although all compositions so far are Ca-dominant.

to a few cubic micrometers if X-ray focusing optics are used, and little sample preparation (e.g., Sutton et al. 2002).

To establish the suitability and sensitivity of XANES spectroscopy as a method of measuring the oxidation state of Te, it is necessary to establish that variation in coordination geometry and intermediate-range structure have a small effect on the XANES spectrum compared to changes in oxidation states. Thus, we measured several telluride, tellurite, and tellurate minerals and inorganic compounds of known structure.

Spectra were collected on beamline 9-BM-B at the Advanced Photon Source (APS) at Argonne National Laboratory, Illinois. Beamline 9-BM-B has a Si (111) monochromator, resulting in an energy resolution $\Delta E/E$ of 1.4×10^{-4} at 10 keV with a flux of 10^{11} photons/s at 15 keV. The beam was focused to a size of 1×1 mm by the use of a rhodium-coated torroidal mirror. A liquid-N_2 cooled 7 element Ge fluorescence detector was located at ~90°

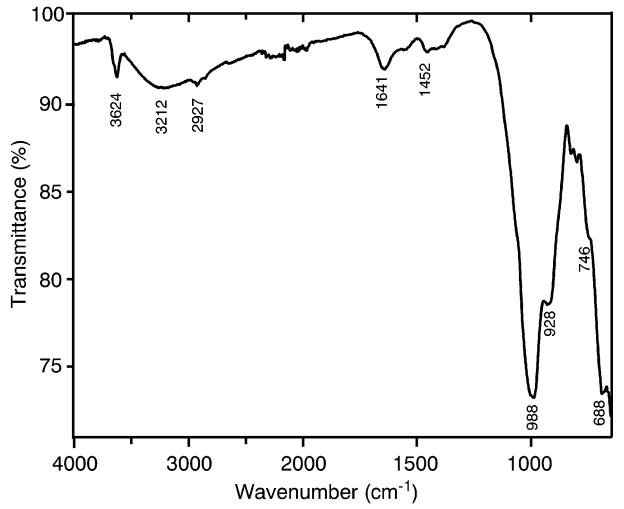

FIGURE 3. FTIR spectrum of xocolatlite showing the presence of small amounts of H_2O as water groups in xocolatlite (3212 cm^{-1} O-H stretching and 1641 cm^{-1} H-O-H binding). The other bands are due to other types of bonds in the structure of the mineral. Scale below 2000 cm^{-1} has been expanded.

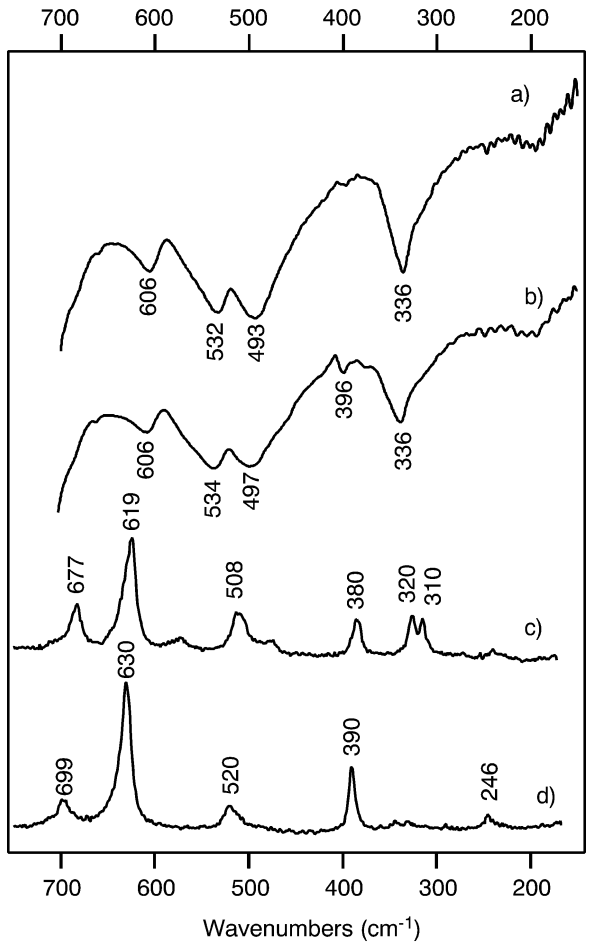

FIGURE 4. FTIR (top) and Raman (bottom) spectra of (**a**,**c**) kuranakhite and (**b**,**d**) xocolatlite, for tentative assignment of bands see text.

to minimize detection of the scattered X-ray beam and an ion chamber was located after the sample for simultaneous collection of transmission data whenever possible. XANES spectra were measured by scanning the energy over the Te-L_{III} absorption edge (4341 eV) while collecting counts in a region of interest centered on the Te$L\alpha_1$ peak (3768 eV). Given the low energy of the Te-L_{III} edge, the beam path and sample chamber were continuously flushed by a stream of He. Data were collected in steps of 0.2 eV from 4320 to 4390 eV with a counting time of 1 s at each step. The monochromator energy was calibrated by defining the first inflection point of the derivative spectrum of powdered Te (99.997%, ~30 mesh, Aldrich) to be 4341 eV. Spectra were collected on this sample at regular intervals during the experiment to confirm the stability of the monochromator.

Samples were finely ground and spread on "Scotch Magic" tape (3M), which was supported on an aluminum sample holder. The identity of the minerals used for analytical work was confirmed by qualitative chemical analysis using an energy dispersive spectrometer mounted on an electron microscope and by powder X-ray diffraction (Gandolfi camera, diameter 114.6 mm with Cu$K\alpha$ radition). Mineral samples were obtained from the collections of the Musée Cantonal de Géologie, Lausanne and the South Australian Museum, Adelaide. Telluric acid (H_6TeO_6, 99.5%) and TeO_2 (99.999%) were purchased from Strem Chemicals, Newburyport (Massachusetts).

Tellurium L_{III}-edge spectra of tellurides and native tellurium are characterized by a small pre-edge feature (maximum at 4337 eV on first derivative) followed by a relatively featureless post-edge region (Fig. 5, bottom). In contrast, the pre-edge peak is well-resolved in tellurites and tellurates, which also show several peaks beyond the edge. The pre-edge feature in Te L_{III}-edge spectra has been ascribed to interactions between the inner $2p_{3/2}$ electrons and the empty Te 5*s* shells (Ibanez et al. 1994), although recent ab-initio calculations by Jiang and Spence (2004) suggest that this feature reflects mainly transitions to empty 5*d* orbitals. The XANES spectra in Figure 5 clearly demonstrate the sensitivity of the L_{III}-edge to the valence state of tellurium. In particular, the energy of the pre-edge allows for unambiguous distinction among tellurate, tellurites, and tellurides for all the analyzed compounds (Fig. 6). The edge energy increases with increasing oxidation state due to an enhancement of the effective nuclear charge as the valence electrons are removed. The same behavior has been reported for sulfur (Li et al. 1995) and selenium (Pickering et al. 1995). Thus, XANES is an efficient method in determining the oxidation state of Te. In the present case, it shows clearly that xocolatlite, and also kuranakhite, contain Te^{6+} (Fig. 6).

It is interesting to note that there is very little difference between the spectra of the four tellurates measured here (Fig. 5). In particular, the positions of all three main peaks are nearly identical. The slight differences in peak width and relative intensities may in part be related to non-optimal sample preparation (due to limited material) and to the experimental conditions. In contrast, the spectra of the measured tellurites (Fig. 5) show significant differences in the number, position, and relative intensity of the peaks present. These differences may be explained by comparing the distribution of Te-O bond lengths for Te^{4+}- and Te^{6+}-bearing minerals. All Te-O bonds for Te^{6+} minerals with known structures

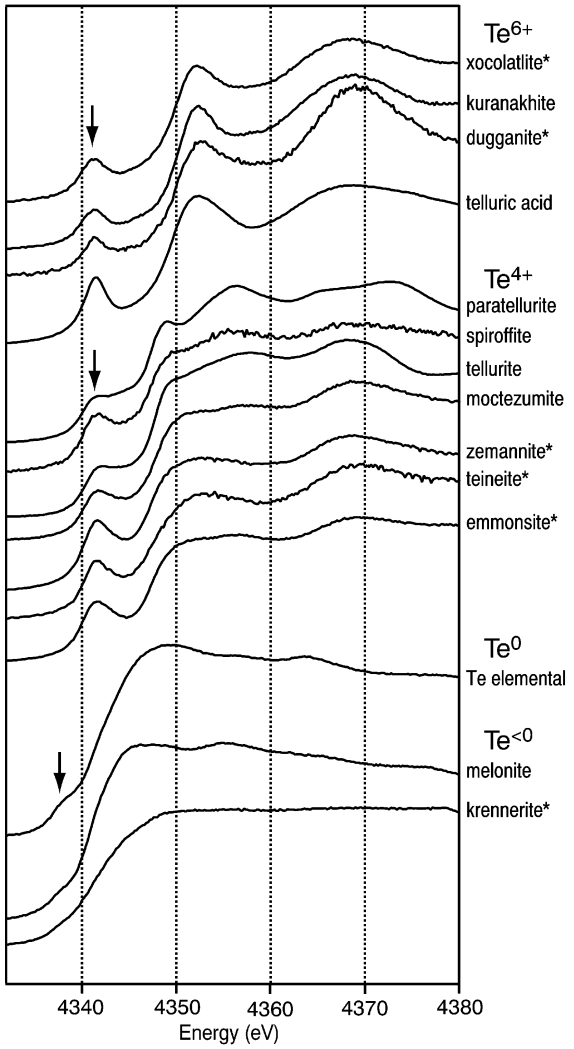

FIGURE 5. Normalized transmission and fluorescence XANES spectra collected from solid samples of Te-containing minerals and synthetic materials. Species fall clearly into three groups: Te^{6+} (xocolatlite, kuranakhite, dugganite, and telluric acid H_6TeO_6), Te^{4+} (paratellurite, spiroffite, tellurite, moctezumite, zemannite, teineite, and emmonsite), and tellurides including the elemental form (tellurium, melonite, and krennerite). Arrows indicate the approximate positions of the pre-edge peaks. * indicate fluorescence spectra.

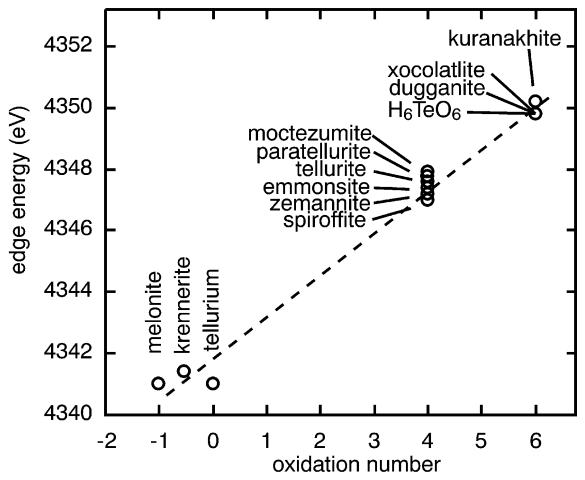

FIGURE 6. Plot showing the relationship between Te-L_{III} edge energy (taken from first derivative plots of the XANES spectra) and Te oxidation number for a selection of tellurium-bearing minerals.

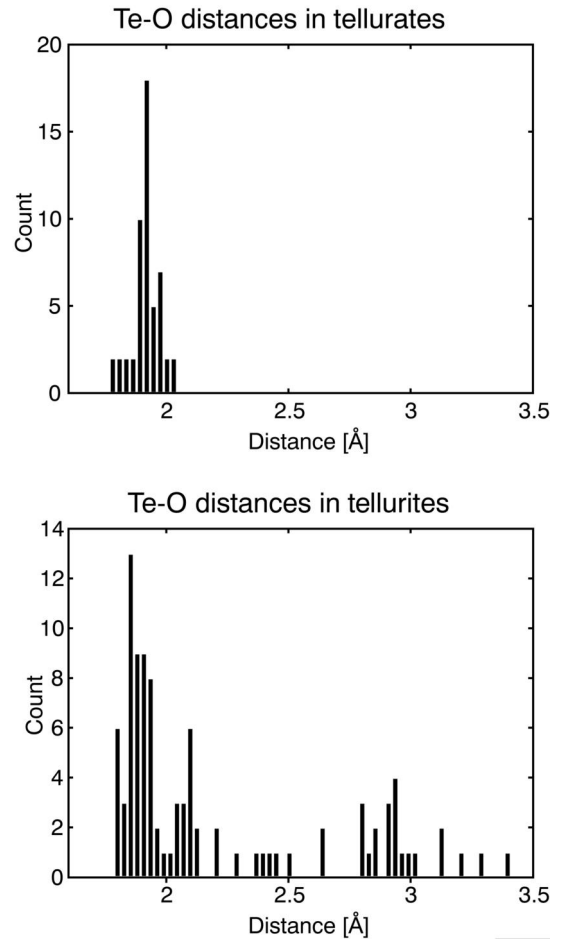

FIGURE 7. Te-O bond distances in tellurites and tellurates (minerals and a few inorganic compounds) included in the Inorganic Crystal Structures Database (ICSD). The spread is much greater for tellurites (coordination numbers 3 to 4) than for tellurates (coordination number 6).

range between 1.74 and 2.04 Å, with an average bond distance of 1.92 Å. This reflects the relatively rigid nature of the TeO_6^{6-} octahedron, the only structural unit found in natural tellurates. In contrast, the Te-O bond distances for Te^{4+} minerals vary across a much wider range, with bonds from 1.78 to 3.41 Å (Fig. 7) and an average bond distance of 2.20 Å. The coordination of Te^{4+} in these compounds varies from 3, to 3 + 1, to 4 O neighbors. Jiang and Spence (2004) demonstrate that the differences, in particular the intensity of the pre-edge peak, observed between XANES spectra of compound with different coordination around the Te^{4+} central atom are sensitive not only to the 3 or 4 nearest neighbors, but to the structure of a cluster 5–8 Å in diameter. This illustrates the importance of measuring a range of standards

to establish the suitability of XANES spectroscopy as a tool to retrieve the oxidation state of Te in minerals.

Chemical formula and relation to other species

The presence of Te^{6+} in xocolatlite shows that the formation of this mineral must have occurred in a highly oxidizing environment, in the presence of free oxygen or another strong oxidant (Fig. 8). Under these conditions Mn is very insoluble and will precipitate as a Mn^{4+} oxide/hydroxide unless the pH is highly acidic, in which case Mn^{2+} is stable in the aqueous phase (Fig. 8). Thus to establish the empirical formula for xocolatlite it was assumed that Mn is present as Mn^{4+}. This assumption is further supported by the dark color of xocolatlite, and is consistent with the average volume per atom of oxygen in the xocolatlite unit cell (Table 3). For the proposed hydrated chemical formula of xocolatlite, the calculated volume per oxygen atom (17.8 Å^3) compares well with that of hydrated tellurates, such as frankhawthorneite and parakhinite (Table 3). An anhydrous formula with Mn^{2+} would lead to the unreasonably high value of 23.2 Å^3.

Since IR spectroscopy showed the presence of a small amount of water (see above), the H_2O content was calculated to obtain 1 H_2O per formula unit (pfu). Thus the empirical formula (based on 6 cations pfu, and assuming all Mn as tetravalent) is

$Ca_{1.262}Zn_{0.193}Pb_{0.118}Al_{0.040}Fe_{0.004}Cd_{0.004}Bi_{0.002}Mn_{2.353}Te_{2.011}S_{0.010}Se_{0.002}O_{12.421}\cdot H_2O$.

This formula can be simplified to $(Ca,Zn,Pb,Mn)_2Mn^{4+}_2Te^{6+}_2O_{12}\cdot H_2O$. The proposed ideal formula is $Ca_2Mn^{4+}_2Te^{6+}_2O_{12}\cdot H_2O$, which requires CaO 17.12, MnO_2 26.54, TeO_3 53.60, H_2O 2.75, total 100.00 wt%.

It should be noted that the inclusion of structural water in xocolatlite is only tentative at this stage. Kuranakhite was reported to be anhydrous, although H_2O was not measured directly and the provided chemical analysis is the average of only 3 EMP analyses (Yablokova et al. 1975). We cannot totally exclude the possibility that the H_2O visible on the IR spectrum of xocolatlite may be related to some extent to contamination, because the material is fine grained, and may still contain some hydrated gel. The consistently low EMP totals may be related to analytical difficulties, e.g., empty spaces between the fibers.

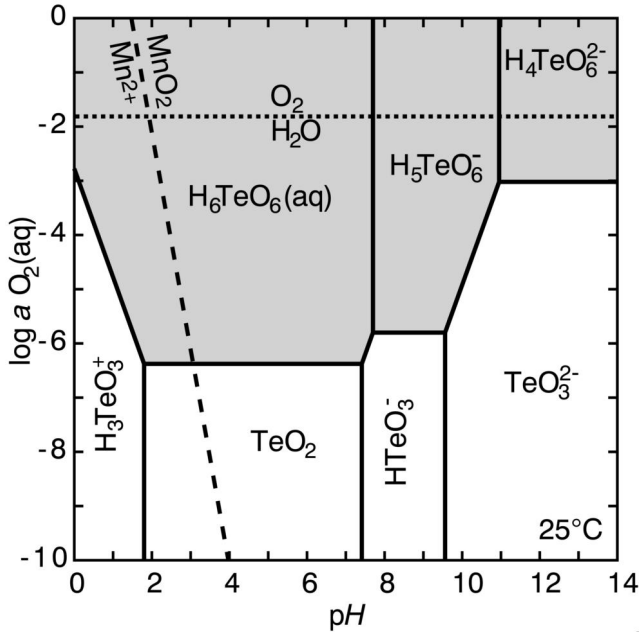

Figure 8. Stability diagram for oxidized Te species. Solid lines are the boundaries of the stability domains of the Te species. Shaded area corresponds to the stability of Te^{6+}. Dashed line represents the boundary between the stability fields of Mn^{2+} and Mn^{4+}, whereas the dotted line represents the limit of water stability toward oxidation. Diagram has been drawn assuming $P = 1.013$ bar, $T = 25$ °C, and activities of Te and Mn equal to 0.0001. Thermodynamic data for Te species from McPhail (1995) and for all other species from the Lawrence Livermore database (LLNL V8 R6), as delivered with the Geochemist's Workbench software (Bethke 1996).

Comparison between the wt% derived from the ideal formula and the actual results from the analyses show a lower Ca content than expected. However the Pb, Fe, and Zn contents are in the

Table 3. Mean volumes of oxygen atoms in some tellurites and tellurates

Mineral	Chemical formula	Cell volume (Å^3)	Z	V_O* (Å^3)	Reference
		Tellurites			
Carlfriesite	$CaTe^{4+}_3O_8$	645.0	4	20.2	Effenberger et al. 1978
Denningite	$(Mn^{2+},Ca,Zn)[Te^{4+}_2O_5]$	1014.4	8	25.4	Walitzi 1965
Mroseite	$CaTe^{4+}O_2CO_3$	827.0	8	20.7	Fischer et al. 1975
Spiroffite	$(Mn,Zn)_2Te^{4+}_3O_8$	814.9	4	25.5	Cooper and Hawthorne 1996
		Tellurates			
"Telluric acid"	$H_2Te^{6+}O_4$	132.7	2	16.6	Moret et al. 1974
Dugganite	$Pb_3(Zn,Cu)_3(Te^{6+}O_6)AsO_4(OH)_3$	322.7	1	24.8	Lam et al. 1998
Frankhawthorneite	$Cu_2[(OH)_2\|Te^{6+}O_4]$	215.6	2	18.0	Grice and Roberts 1995
Jensenite	$Cu^{2+}_2Te^{6+}O_6\cdot 2H_2O$	628.6	4	19.6	Grice et al. 1996
Khinite	$PbCu^{2+}_3Te^{6+}O_6(OH)_2$	1373.0	8	21.5	Burns et al. 1995
Leisingite	$Cu(Mg,Cu,Fe,Zn)_2[Te^{6+}O_6]\cdot 6H_2O$	237.9	1	19.8	Margison et al. 1997
Parakhinite	$Cu^{2+}_3PbTe^{6+}O_4(OH)_6$	517.2	3	17.2	Burns et al. 1995
Yafsoanite	$Ca_3Zn_3[Te^{6+}O_6]_2$	2015.7	8	21.0	Jarosch and Zemann 1989
Kuranakhite	$PbMn^{4+}Te^{6+}O_6$	240.6	1	18.5	Yablokova et al. 1975
Xocolatlite	$Ca_2Mn^{4+}_2Te^{6+}_2O_{12}\cdot H_2O$	463.0	2	17.8	This work
Xocolatlite (anhydrous)	$Ca_2Mn^{4+}_2Te^{6+}_2O_{12}$	463.0	2	19.3	This work
Xocolatlite (with Mn^{2+})	$Ca_2Mn^{2+}_2Te^{6+}_2O_{10}$	463.0	2	23.2	This work

* Volume per oxygen atom.

TABLE 4. Ca- and Mn-bearing tellurites and tellurates

Mineral	Chemical formula	Unit cell (Å, °)	M/Te	Space group
Xocolatlite	$Ca_2Mn^{4+}_2Te^{6+}_2O_{12}{\cdot}H_2O$	a = 10.757, b = 4.928, c = 8.942, β = 102.39	2	*Pm P2 P2/m*
Kuranahkite	$PbMn^{4+}Te^{6+}O_6$	a = 5.1, b = 8.9, c = 5.3	2	*P2 P2/m*
Carlfriesite	$CaTe^{4+}_2Te^{6+}O_8$	a = 12.576, b = 5.662, c = 9.994, β = 115.56	1/3	*C*
Denningite	$(Ca,Mn^{2+})(Mn^{2+},Zn)Te^{4+}_4O_{10}$	a = 8.82, c = 13.04	1/2	*C2/c*
Mroseite	$CaTe^{4+}O_2(CO_3)$	a = 6.988, b = 11.201, c = 10.566	1	*Pbca*
Spirroffite	$(Mn^{2+},Zn)_2Te^{4+}_3O_8$	a = 12.870, b = 5.381, c = 11.888, β = 98.22	2/3	*C2/c*
Yafsoanite	$(Ca,Pb)_3Zn_3Te^{6+}_2O_{12}$	a = 12.632	3	*Ia3d*

percent range and may substitute for calcium. Furthermore, the negative correlation between Mn and the sum of Ca-site cations (Ca, Fe, Zn, Pb) as shown in Figure 2c indicate a possible substitution by Mn^{2+} (possibly also Mn^{3+}) on the Ca site. This also explains the higher Mn contents in the actual analyses compared to the ideal formula. The presence of a fraction of Mn under a lower oxidation state also eliminates the excess of oxygen calculated in the formula unit (i.e., 13.4 O pfu instead of the theoretical 13.0 pfu).

Chemically, xocolatlite is related to the Ca- or Mn-bearing tellurites/tellurates listed in Table 4. The metal to tellurium ratios indicate a relationship between xocolatlite and kuranakhite, $PbMnTeO_6$ (Yablokova et al. 1975).

Comparison of the X-ray powder-diffraction patterns of both minerals reveals that they are indeed related (Table 5), although there are significant differences: for example, there is no exact match for the most intense kuranakhite line at ~3.4 Å in xocolatlite, but it may well correspond to the 3.267 Å line in the synchrotron data. The inconsistencies in the intensities of the X-ray diffraction lines obtained from Guinier and synchrotron measurements are most probably due to preferential orientation and possibly to absorption effects. The sample was flat for the Guinier measurement (spread over sticky tape), while the synchrotron sample was contained in a 0.3 mm internal diameter glass capillary. The cell volume of xocolatlite is about twice of that reported for kuranakhite (Table 3). Striking similarities of the Raman and IR spectra are also indicative of a relation between these two minerals (Fig. 5).

The validity of xocolatlite as a new mineral species distinct from kuranakhite relies upon the assumption that Ca and Mn occur in different crystallographic sites. In the absence of a crystal-structure refinement, crystal-chemical considerations are used to assess that this is the case. Both kuranakhite and xocolatlite contain Te^{6+}, which occurs only under very oxidizing conditions favoring the presence of Mn^{4+}. Knowing that Mn^{4+} and Ca^{2+}/Pb^{2+} have very different ionic radii, they most likely occur on different crystallographic sites. This is further supported by the fact that kuranakhite is highly stoichiometric (Table 2), with (Pb + Ca)/Mn ratios between 0.89 and 1.04, indicating that Ca + Pb are very likely to occupy a different crystallographic site than Mn. Figure 2e shows that kuranakhite and xocolatlite have very distinct compositions in the Ca-Pb-Fe space resulting in the occurrence of nearly pure end-members. The identity of xocolatlite as a separate mineral species is also suggested by the significant differences in the XRD patterns of the two minerals, which may be connected with the ordering of Mn and Ca/Pb (Table 5). In the Strunz classification (Strunz and Nickel 2001), xocolatlite should be placed together with kuranakhite, e.g., in 4.DM.25., as an "oxide with large (±medium sized) cations; unclassified," until crystal structural work possibly allows a more precise classification.

TABLE 5. Comparison of X-ray diffraction data for xocolatlite and kuranakhite (diffraction data from Guinier films was chosen for comparison because they were recorded under similar conditions)

	Xocolatlite* Guinier, Cr*K*α		Kuranakhite* Guinier, Cr*K*α		Kuranakhite JCPDS 29-779 Cu*K*α		
hkl	*d* (Å)	I/I_{max}	*d* (Å)	I/I_{max}	*hkl*	*d* (Å)	I/I_{max}
010	4.930	0.02 (F)	5.302	1			
002	4.374	0.15 (F)	4.393	26			
			3.411	51	111	3.4	100
			3.381	60			
012	3.269	64	3.277	4			
			2.703	9			
			2.658	6			
$30\bar{3}$	2.523	100	2.534	100	130	2.558	60
$41\bar{1}$	2.352	7	2.465	12			
			2.302	5	131	2.322	10
004	2.183	7	2.194	33	220	2.205	5
			2.058	4			
014	1.998	28	2.038	33	410	2.05	50
?	1.892	5	2.027	50			
			1.851	24	132	1.851	50
$32\bar{3}/60\bar{2}$	1.763	35	1.835	30			
512/601/610	1.651	11	1.687	3			
611	1.566	27	1.668	6	310	1.668	10
?	1.488	3	1.658	7			
$01\bar{6}$	1.397	12			241	1.596	40
$60\bar{6}$	1.260	12			330	1.475	5
					043	1.388	5

* Diffraction data collected using a 100 mm diameter Guinier-Hägg camera under a slight vacuum with Cr*K*α radiation (λ = 2.28970 Å). The sample material and NIST Si, as an internal standard, were spread on sticky tape for data collection. Photographic film was used as detector. After development, it was digitized using an optical scanner. The 2θ scale was calibrated by a linear regression based on the four most intense Si lines.

ACKNOWLEDGMENTS

P.G. thanks D. Baumann from the Institut des sciences et ingénierie chimiques, Ecole Polytechnique Fédérale de Lausanne (Switzerland) for his assistance during the recording of the IR spectra. This work has been funded in part by grant LP0454976, financed by the Australian Research Council, Anglo-Gold Ashanti, The South Australian Museum, and Primary Industry and Resources South Australia (PIRSA). Synchrotron work was supported by the Access to Major Research Facilities Program, which is a component of the International Science Linkages Program established under the Australian Government's innovation statement, Backing Australia's Ability. Use of the Advanced Photon Source was supported by the U.S. Department of Energy, Office of Science, Office of Basic Energy Sciences, under contract no. DE-AC02-06CH11357. We thank the Swiss-Norwegian Beamline (H. Emerich and W. van Beek) for providing beam time. Thanks to Sergey Krivovichev for attempting to measure a single crystal at the ESRF. Helpful comments from S. Mills, an anonymous referee and the editor, I. Swainson, are acknowledged.

REFERENCES CITED

Bateman, R. and Hagemann, S. (2004) Gold mineralization throughout about 45 Ma of Archaean orogenesis: Protracted flux of gold in the Golden Mile, Yilgarn craton, Western Australia. Mineralium Deposita, 39, 536–559.

Bethke, C.M. (1996) Geochemical reaction modeling, concepts and applications, 397 p. Oxford University Press, New York.

Boultif, A. and Louer, D. (1991) Indexing of powder diffraction patterns for low-symmetry lattices by the successive dichotomy method. Journal of Applied

Crystallography, 24, 987–993.
Braith, H., Gröbner, J., Langer, G., and Seitz, M. (2001) Moctezumas geheime Schätze: Bambolla, Bambollita und San Miguel. Lapis, 26, 11–23.
Burns, P.C., Cooper, M.A., and Hawthorne, F.C. (1995) Parakhinite, $Cu^{2+}_{3}PbTe^{6+}O_6(OH)_2$; crystal structure and revision of chemical formula. The Canadian Mineralogist, 33, 33–40.
Charton, P. and Armand, P. (2004) X-ray absorption and Raman characterizations of TeO_2-Ga_2O_3 glasses. Journal of Non-Crystalline Solids, 333, 307–315.
Ciobanu, C.L., Cook, N.J., Damian, G., Damian, F., and Buia, G. (2004) Telluride and sulfosalt associations at Săcărîmb. IAGOD Guidebook Series, 12, 145–186.
Cooper, M.A. and Hawthorne, F.C. (1996) The crystal structure of spiroffite. The Canadian Mineralogist, 34, 821–826.
Deen, J.A. and Atkinson, W.W.J. (1988) Volcanic stratigraphy and ore deposits of the Moctezuma district, Sonora, Mexico. Economic Geology, 83, 1841–1855.
Effenberger, H., Zemann, J., and Mayer, H. (1978) Carlfriesite: Crystal structure, revision of chemical formula, and synthesis. American Mineralogist, 63, 847–852.
Ferraro, J.R. (1971) Low-frequency vibrations of inorganic and coordination compounds, 309 p. Plenum Press, New York.
Fischer, R., Pertlik, F., and Zemann, J. (1975) The crystal structure of mroseite, $CaTeO_2(CO_3)$. The Canadian Mineralogist, 13, 383–387.
Grice, J.D. and Roberts, A.C. (1995) Frankhawthorneite, a unique Hcp framework structure of a cupric tellurate. The Canadian Mineralogist, 33, 649–653.
Grice, J.D., Groat, L.A., and Roberts, A.C. (1996) Jensenite, a cupric tellurate framework structure with two coordinations of copper. The Canadian Mineralogist, 34, 55–59.
Ibanez, A., Ericsson, T., Lindqvist, O., Bazin, D., and Philippot, E. (1994) Local range order of tellurium atoms in TeO_2-BaO and TeO_2-BaF_2 glassy systems. Journal of Material Chemistry, 4, 1101–1106.
Jarosch, D. and Zemann, J. (1989) Yafsoanite: A garnet type calcium-tellurium(VI)-zinc oxide. Mineralogy and Petrology, 40, 111–116.
Jiang, N. and Spence, J.C.H. (2004) Intermediate-range structure of tellurite glasses from near-edge absorption spectra. Physical Review B (Condensed Matter and Materials Physics), 70, 184113.
Kelley, K.D., Romberger, S.B., Beaty, D.W., Pontius, J.A., Snee, L.W., Stein, H.J., and Thompson, T.B. (1998) Geochemical and geochronological constraints on the genesis of Au-Te deposits at Cripple Creek, Colorado. Economic Geology, 93, 981–1012.
Lam, A.E., Groat, L.A., and Ercit, T.S. (1998) The crystal structure of dugganite, $Pb_3Zn_3Te^{6+}As_2O_{14}$. The Canadian Mineralogist, 36, 823–830.
Li, D., Bancroft, M., Kasrai, M., Fleet, M.E., Feng, X., and Kim, T. (1995) S *K*- and *L*-edge X-ray absorption spectroscopy of metal sulfides and sulfates: applications in mineralogy and geochemistry. The Canadian Mineralogist, 33, 949–960.
Libowitzky, E. and Rossman, G.R. (1997) An IR absorption calibration for water in minerals. American Mineralogist, 82, 1111–1115.
Liegeois-Duyckaerts, M. (1975) Vibrational studies of molybdates, tungstates, and related compounds—IV. Hexagonal perovskites: $Ba_2B^{II}TeO_6$ (B^{II} = Ni, Co, Zn). Spectrochimica Acta, 31A, 1585–1588.
Margison, S.M., Grice, J.D., and Groat, L.A. (1997) The crystal structure of leisingite, $(Cu^{2+},Mg,Zn)_2(Mg,Fe)Te^{6+}O_6{\cdot}6H_2O$. The Canadian Mineralogist, 35, 759–763.
McPhail, D.C. (1995) Thermodynamic properties of aqueous tellurium species between 25 and 350 °C. Geochimica Cosmochimica Acta, 59, 851–866.
Miletich, R. (1995) Crystal chemistry of the microporous tellurite minerals zemannite and kinichilite, $Mg_{0.5}[Me^{2+}Fe^{3+}(TeO_3)_3]{\cdot}4.5H_2O$, ($Me^{2+}$ = Zn,Mn). European Journal of Mineralogy, 7, 509–523.
Moret, J., Philippot, E., Maurin, M., and Lindqvist, O. (1974) Structure cristalline de l'acide tetraoxotellurique H_2TeO_4. Acta Crystallographica Section B, 30, 1813–1818.
Novak, A. (1974) Hydrogen bonding in solids. Correlation of spectroscopic and crystallographic data. Structure and Bonding, 18, 177–216.
Pals, D.W. and Spry, P.G. (2003) Telluride mineralogy of the low-sulfidation epithermal Emperor gold deposit, Vatukoula, Fiji. Mineralogy and Petrology, 79, 285–307.
Pickering, I.J., Brown, G.E., and Tokunaga, T.K. (1995) Quantitative speciation of selenium in soils using X-ray absorption spectroscopy. Environmental Science and Technology, 29, 2456–2459.
Roberts, A.C., Ercit, T.S., Criddle, A.J., Jones, G.C., Williams, R.S., Cureton, F.F.I., and Jensen, M.C. (1994) Mcalpineite, $Cu_3TeO_6{\cdot}H_2O$, a new mineral from the McAlpine mine, Tuolumne county, California, and from the Centennial Eureka mine Juab county, Utah. Mineralogical Magazine, 58, 417–424.
Roberts, A.C., Grice, J.D., Criddle, A.J., Jensen, M.C., Harris, D.C., and Moffatt, E.A. (1995) Frankhawthorneite, $Cu_2Te^{6+}O_4(OH)_2$, a new mineral species from the Centennial Eureka Mine, Tintic District, Juab County, Utah. The Canadian Mineralogist, 33, 641–647.
Roberts, A.C., Grice, J.D., Groat, L.A., Criddle, A.J., Gault, R.A., Erd, R.C., and Moffatt, E.A. (1996a) Jensenite, $Cu_3Te^{6+}O_6{\cdot}2H_2O$, a new mineral species from the Centennial Eurek Mine, Tintic District, Juab County, Utah. The Canadian Mineralogist, 34, 49–54.
Roberts, A.C., Groat, L.A., Grice, J.D., Gault, R.A., Jensen, M.C., Moffatt, E.A., and Stirling, J.A.R. (1996b) Leisingite, $Cu(Mg,Cu,Fe,Zn)_2Te^{6+}O_6{\cdot}6H_2O$, a new mineral species from the Centennial Eureka mine, Juab county, Utah. Mineralogical Magazine, 60, 653–657.
Roberts, A.C., Gault, R.A., Jensen, M.C., Criddle, A.J., and Moffatt, E.A. (1997) Juabite, $Cu_5(Te^{6+}O_4)_2(As^{5+}O_4)_2{\cdot}3H_2O$, a new mineral species from the Centennial Eureka Mine, Juab County, Utah. Mineralogical Magazine, 61, 139–144.
Shackleton, J.M., Spry, P.G., and Bateman, R. (2003) Telluride mineralogy of the Golden Mile deposit, Kalgoorlie, Western Australia. The Canadian Mineralogist, 41, 1503–1524.
Strunz, H. and Nickel, E.H. (2001) Strunz Mineralogical Tables, 870 p. E. Schweizerbart'sche Verlagsbuchhandlung, Stuttgart.
Sung, Y.H., Ciobanu, C.L., Pring, A., Brugger, J., Skinner, W., Cook, N.J., and Nugus, M. (2007) Tellurides from Sunrise Dam gold deposit, Yilgarn Craton, Western Australia: a new occurrence of nagyágite. Mineralogy and Petrology, 91, 249–270.
Sutton, S.R., Bertsch, P.M., Newville, M., Rivers, M., Lanzirotti, A., and Eng, P. (2002) Microfluorescence and microtomography analyses of heterogeneous Earth and Environmental materials. In P. Fenter, M. Rivers, N. Sturchio, S. Sutton, Eds., Applications of Synchrotron Radiation in Low-Temperature Geochemistry and Environmental Science, 49, p. 429–483. Reviews in Mineralogy and Geochemistry, Mineralogical Society of America, Chantilly, Virginia.
Walitzi, E.M. (1965) Die Kristallstruktur von Denningit, $(Mn,Ca,Zn)Te_2O_5$; Ein Beispiel fur die Koordination um vierwertiges Tellur. Tschermak's Mineralogische und Petrographische Mitteilungen, 10, 241–255.
Yablokova, S.V., Dubakina, L.S., Dmitrik, A.L., and Sokolova, G.V. (1975) Kuranakhite, a new supergene tellurium mineral. Zapiski Vsesoyuznogo Mineralogicheskogo Obshchestva, 104, 310–313 (in Russian).

MANUSCRIPT RECEIVED NOVEMBER 27, 2007
MANUSCRIPT ACCEPTED MAY 28, 2008
MANUSCRIPT HANDLED BY IAN SWAINSON